# Multimodal Energy Harvesting System: Piezoelectric and Electromagnetic

YONAS TADESSE,[1] SHUJUN ZHANG[2] AND SHASHANK PRIYA[1,*]

[1]*CIMSS, Department of Mechanical Engineering, Virginia Tech, Blacksburg VA, 24061, USA*

[2]*Materials Research Institute, Penn State, University Park, PA 16802, USA*

**ABSTRACT:** In this study, we report a multimodal energy harvesting device that combines electromagnetic and piezoelectric energy harvesting mechanism. The device consists of piezoelectric crystals bonded to a cantilever beam. The tip of the cantilever beam has an attached permanent magnet which, oscillates within a stationary coil fixed to the top of the package. The permanent magnet serves two purpose (i) acts as a tip mass for the cantilever beam and lowers the resonance frequency, and (ii) acts as a core which oscillates between the inductive coils resulting in electric current generation through Faraday's effect. Thus, this design combines the energy harvesting from two different mechanisms, piezoelectric and electromagnetic, on the same platform. The prototype system was optimized using the finite element software, ANSYS, to find the resonance frequency and stress distribution. The power generated from the fabricated prototype was found to be 0.25 W using the electromagnetic mechanism and 0.25 mW using the piezoelectric mechanism at 35 g acceleration and 20 Hz frequency.

*Key Words:* piezoelectric, electromagnetic, energy harvesting, PZN-PT, resonance, single crystal.

## INTRODUCTION

THERE has been continuous focus on developing small-integrated-smart structures for energy harvesting in various defense and civil applications. Research efforts in this arena have focused on present generation structural health monitoring systems, hybrid automobiles, wireless sensor networks, and domestic tools and appliances (Sodano et al., 2004; Anton and Sandano, 2007; Priya, 2007). Previously, solar energy, hydrogen fuel cell, thermoelectric devices, and wind mills have been used as methods for generating energy. However, integration of these methods with intended platforms of 'small-power range energy-on-demand' is expensive, tedious and technology driven. Piezoelectric devices have shown high potential for vibration energy harvesting, however, they work effectively only under a large stress. An improved piezoelectric cymbal of 29 mm diameter and 1 mm thickness under a force of 7.8 N can generate 39 mW power output across a 400 KΩ resistor at a frequency of 100 Hz (Kim et al., 2007). However, it is difficult to further increase the preload to obtain larger power output, because the stress level is limited by material's mechanical breakdown strength. In order to effectively harvest higher power levels, a multimodal methodology is required.

In a wireless sensor network, self-powering of sensor nodes can be achieved by developing smart architecture which utilizes all the environmental resources available for generating electrical power. These resources can be structural vibrations, wind, magnetic fields, light, sound, temperature gradients and water currents. The generated electric energy is stored in matching media selected by microprocessor depending upon the power magnitude and output impedance (Williams and Yates, 1996; Poulin et al., 2004; Raghunathan et al., 2005; Priya, 2005; Rabaey and Verstraete, 2005; Priya et al., 2006). The stored electrical energy is supplied on demand to the sensors and communications devices. Building upon this concept, in this study we investigate the design and performance of a combinatory energy harvester that demonstrates enhanced power density for a mechanical energy harvesting system.

Figure 1 shows the schematic of prototype device. The harvester consists of a permanent magnet attached at the tip of a cantilever beam which has tapered cross-sectional area. Three piezoelectric single crystal plates were bonded on both top and bottom of the beam. The piezoelectric plates were isolated from beam by using an insulating epoxy. The output voltages of top and bottom row of piezoelectric were connected in parallel as shown in Figure 1. A stationary inductive coil was attached to the

*Author to whom correspondence should be addressed.
E-mail: spriya@vt.edu
Figures 1–7, 9 and 10 appear in color online: http://jim.sagepub.com



1045-389X/09/05 0625–8 $10.00/0 DOI: 10.1177/1045389X08099965

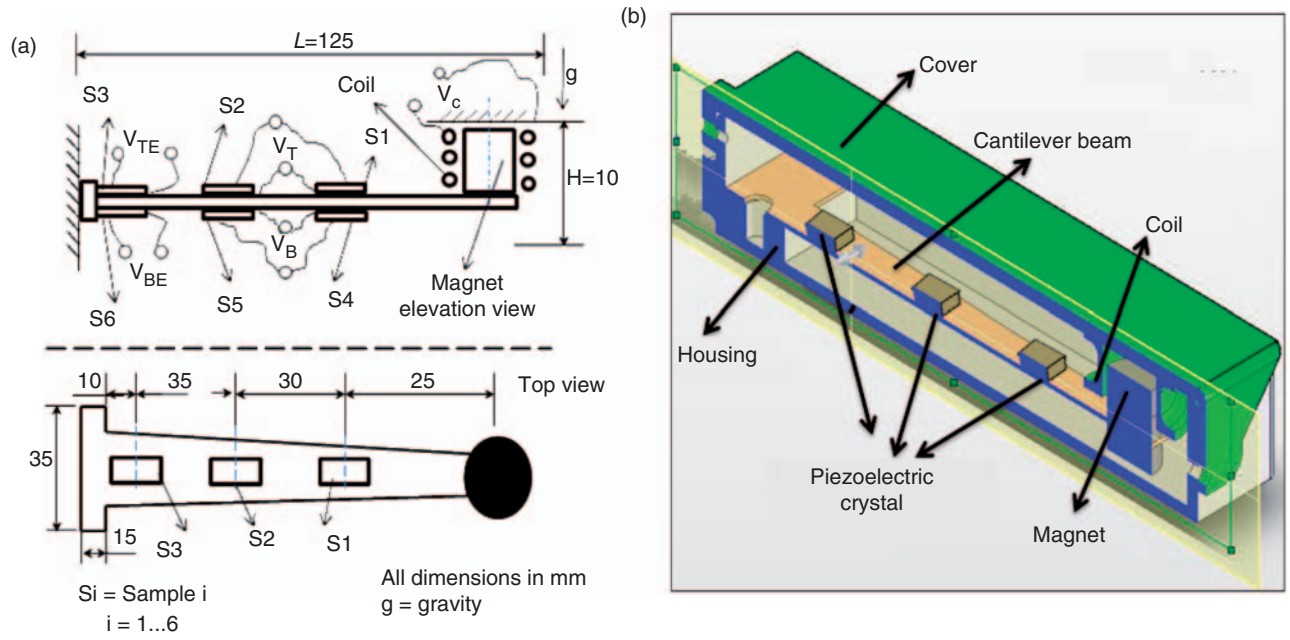


***Figure 1.*** *(a) Isometric view of multimodal prototype mechanical energy harvester (b) Schematic diagram depicting the placement of piezoelectric plates, magnet and coil in the housing.*

housing such that tip mass of the cantilever beam was co-centric with the coil. As the beam vibrates, the magnet moves in and out of the coil which generates voltage across a load following Faraday's law. The beam has tapered geometry with linear variation in dimension along the length such that it's moment of inertia along the axis perpendicular to the direction of vibration also varies linearly. This allows the beam to exhibit higher sensitivity. When a cantilevered beam is subjected to external excitation, various modes occur at respective resonance frequencies depending upon the geometry, modulus of elasticity, density, and boundary conditions. Here we focus on first two vibration modes as they cover the desired operating range of 20–400 Hz for the dimension of cantilever shown in Figure 1.

The advantage of this design is as following. At constant acceleration, the output power from electromagnetic is much higher at lower frequencies (first transversal resonance mode) while that of piezoelectric is higher at higher frequencies (second transversal resonance mode). This behavior allows obtaining significant magnitude of output power from the same device over a wide operating frequency range.

## FEM AND ANALYTICAL MODELING OF THE MULTIMODAL ENERGY HARVESTER

The optimum location for bonding the piezoelectric plates on cantilever beam was determined by FEM analysis (ANSYS). The modal analysis was conducted by using Block Lanczos modal extraction method and Solid92 element type was applied for both the beam and tip mass. The material properties used for aluminum material were: Young's modulus, $E = 70\,\text{GPa}$; Poison's ratio, $\nu = 0.33$; and density, $\rho = 2700\,\text{kg/m}^3$. The tip mass was modeled by using the parameters as: $E = 110\,\text{GPa}$, $\nu = 0.3$ and $\rho = 8745\,\text{kg/m}^3$. The contours of stress intensity were determined as a function of frequency that provided the information about resonance modes. Figure 2 shows the relative deformation when the cantilever beam was subjected to oscillate at the first and second mode. The natural frequencies obtained from the simulation for first three modes were 19.38, 175, and 265 Hz respectively. The observed second mode was not transversal mode but rather a wobbling mode which may be due to eccentricity of tip mass under the given mesh conditions and thus it is not useful for energy harvesting.

The natural frequency of the beam can be obtained analytically from Equation (1) as:

$$f_i = \frac{1}{2\pi}\left(\frac{yi}{L}\right)^2\sqrt{\frac{EI}{\rho A}} \tag{1}$$

where $i$ is the mode index, and $y_i$ is the mode shape number. For the tip to beam mass ratio of $M/M_v = 3$, the first two modes are given by: $y_1 = 0.98$, $y_2 = 3.964$. If the density of beam is $\rho = 2700\,\text{kg/m}^3$, area $= 16\,\text{mm}^2$, length (L) $= 100\,\text{mm}$, and $E = 70\,\text{GPa}$, then the natural frequency can be calculated to be $f_1 = 22.5\,\text{Hz}$, and $f_2 = 366.8\,\text{Hz}$. The calculated value of the first natural frequency was quite close to that determined from FEM but the second frequency has minor difference. This could be corrected by mesh refinement and placement of the load in the FEM model.

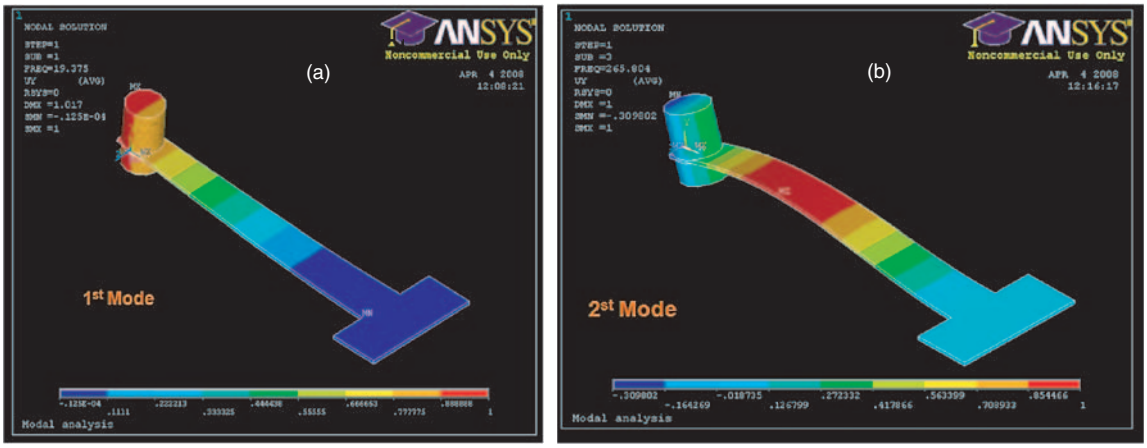


***Figure 2.*** *Mode shapes for tapered beam when subjected to vibration of large tip mass (a) first mode, and (b) second mode.*

Modeling of cantilevered piezoelectric vibration harvester has been analyzed for a beam with a layer of PZT and substrate for various base excitations (Erturk and Inman, 2008). In this article we are interested to find the stress distribution along the beam from the curvature equation. The stress distribution across a cantilever beam loaded at the tip can be estimated from second derivative of the displacement, $w$. Using Figure 3(a), the strain on surface of beam at a distance $y$ from the neutral axis is given by:

$$\varepsilon = -y\frac{\partial^2 w}{\partial x^2} \tag{2}$$

The curvature can be obtained from the fundamental Euler Bernoulli beam equation for the given boundary condition expressed as:

$$EI\frac{\partial^4 w(x,t)}{\partial x^4} = -\lambda_m \frac{\partial^2 w(x,t)}{\partial t^2} \tag{3}$$

where $\lambda_m = \rho A$ is the linear mass density of beam. The change in transverse displacement with respect to position $X(x/L)$ and time $q(t)$ can be obtained by separation of variables, where $x/L$ is the ratio of distance from clamped end to the total length of beam, as following:

$$w_i = C_1 X\left(\frac{x}{L}\right) q(t) \tag{4}$$

The solution of Equation (3) for the tip mass boundary condition described in Figure 1 was given by Laura et al. (1974) as following:

$$X\left(\frac{x}{L}\right) = C_1\left\{\cos\left(\frac{y_i x}{L}\right) - \frac{\cos y_i + \cosh y_i}{\sin y_i + \sinh y_i}\sin\frac{y_i x}{L} - \cosh\frac{y_i x}{L} + \frac{\cos y_i + \cosh y_i}{\sin y_i + \sinh y_i}\sinh\frac{y_i x}{L}\right\} \tag{5}$$

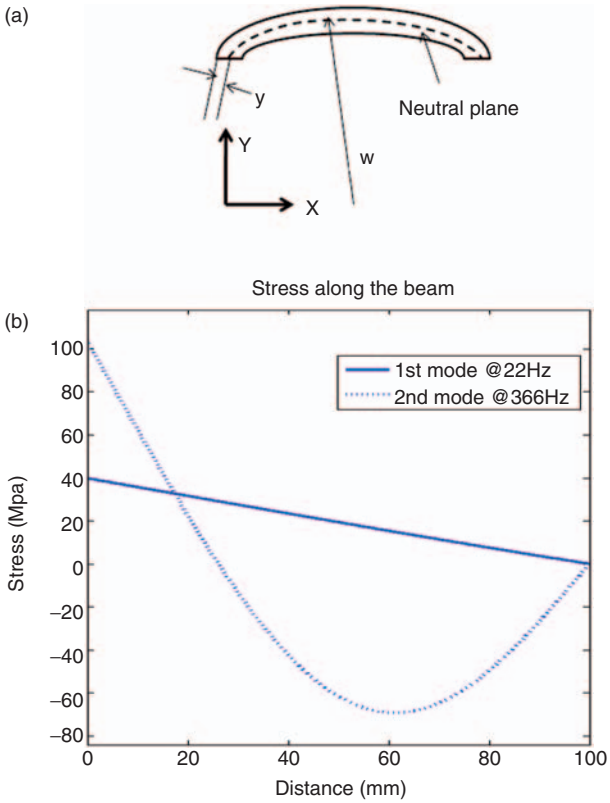


***Figure 3.*** *(a) Schematic depiction of curvature of beam with length L. (b) Stress as a function of distance from the clamped end to length ratio at the first and second resonance frequency.*

where $C_1$ is arbitrary constant, $i$ is the mode index, $y_i$ is the mode shape number and $x$ is the distance from clamped end. The second partial derivative of displacement can be obtained to be:

$$\frac{\partial^2 w_i}{\partial x^2} = C_1\frac{y_i^2}{L^2}q(t)\left\{-\cos\left(\frac{y_i x}{L}\right) - \frac{\cos y_i + \cosh y_i}{\sin y_i + \sinh y_i}\sin\frac{y_i x}{L} - \cosh\frac{y_i x}{L} + \frac{\cos y_i + \cosh y_i}{\sin y_i + \sinh y_i}\sinh\frac{y_i x}{L}\right\} \tag{6}$$

Thus, the maximum surface strain can be obtained by substituting Equation (6) into Equation (2) and using half the beam thickness $h$ as $y$ results:

$$\varepsilon\left(\frac{x}{L}\right) = C_1 h \frac{Y_i^2}{L^2} F_q \left\{ -\cos\left(\frac{y_i x}{L}\right) - \frac{\cos\, y_i + \cosh\, y_i}{\sin\, y_i + \sinh\, y_i} \sin\frac{y_i x}{L} - \cosh\frac{y_i x}{L} + \frac{\cos\, y_i + \cosh\, y_i}{\sin\, y_i + \sinh\, y_i} \sinh\frac{y_i x}{L} \right\} \quad (7)$$

Since we are interested in effect of frequency, the variable $q(t)$ was replaced by $F_q$ in frequency domain and it is solution of ordinary differential equation $m\ddot{q}(t) + c\dot{q}(t) + kq(t) = m\ddot{z}(t)$ in modal coordinate. Assuming static deflection equal to dynamic case at time $t = 0$, a magnitude of 0.5 for constant $C_1$ was utilized. The effect of forcing function $F_q$ was obtained from the equivalent spring mass system for forced vibration with a base excitation given as:

$$F_q = \left| \frac{\omega^2 z_0}{\sqrt{(\omega n_i^2 - \omega^2)^2 + (2\zeta\omega n_i \omega)^2}} \right| \quad (8)$$

where $\omega n_i$ is the natural frequency, $\omega$ is the operating frequency, $\zeta$ is the damping term, and $z_0$ is a unit base excitation. The approximate stress on each section of beam as a function of position to length ratio $(x/L)$ can be obtained from the expression below:

$$\sigma\left(\frac{x}{L}\right) = E\varepsilon\left(\frac{x}{L}\right) \quad (9)$$

where $E$ is the modulus of elasticity of beam material. Figure 3(b) shows the stress distribution as a function of ratio of distance from the clamped end to total length at the first and second resonance frequency. Assuming that the material is linear, elastic and isotropic with an average stress applied along the 1–1 direction, the output voltage can be determined from Equation (10) as:

$$V\left(\frac{x}{L}\right) = g_{31} E\varepsilon\left(\frac{x}{L}\right) L_b \quad (10)$$

The output power as a function of distance $x$ from the clamped end can be expressed as:

$$P = \frac{v^2}{R_L} = \frac{1}{R_L}\left\{ g_{31} E\varepsilon\left(\frac{x}{L}\right) L_b \right\}^2 \quad (11)$$

where $R_L$ is load resistance and $L_b$ is length of piezoelectric crystal. In static case for a free-clamped cantilever with tip mass, the maximum bending moment occurs at the clamped position. For a 17 gm mass and 100 mm length of cantilever, the bending moment can be determined to be: $M = \text{mgL} = 16.6 \times 10^{-3}$ Nm. The flexural stress can be calculated from the expression: $\sigma = \text{Mc/I}$. The moment of inertia can be calculated as: $I = (1/12)\ \text{bh}^3 = 1.33\,\text{mm}^2$, while distance from the neutral plane is given as $c = 0.5$ mm. Thus, the stress can be found to be $\sigma = 6.54$ MPa. The stress along the beam will be much higher in the dynamic case than this value especially at resonance frequency. The stress along the position of the beam $x/L = 0.75$, 0.45, and 0.10 were calculated to be 9, 21, and 35 MPa, respectively, in the first mode of vibration. The maximum voltage generated across the crystal plate can be obtained by using Equation (10). For sample 1 (crystal on top end closer to tip mass), using the values of $\sigma_1^1 = 9.2$ MPa, $g_{31} = 12.66 * 10^{-3}(Vm/N)$ and $L = 7$ mm, the maximum voltage calculated using Equation (10) was 815.3 V. In practice, the output will be damped by a large factor due to damping and mechanical losses.

## EXPERIMENTAL CHARACTERIZATION

The damping constant for the cantilever beam was determined by applying a step input excitation and measuring the amplitude of the resultant displacement. The displacement was measured by using Polytec laser vibrometer (Model OFV3001). Initially, a plot of natural logarithmic amplitude to the $n$-th amplitude was constructed as a function of number of decaying cycles. Assuming the linear variation, the damping can be obtained from following expression:

$$\ln\left|\frac{A_0}{A_1}\right| = \frac{2\pi n\zeta}{\sqrt{(1-\zeta^2)}} \quad (12)$$

where $A_0$ is the first amplitude of signal, $n$ is decaying cycle and $\zeta$ is a damping constant. Figure 4(a) shows the measured displacement for a step input excitation and Figure 4(b) shows the measured data along with assumption of linear variation. The damping coefficient was found to be $\zeta = 0.0423$ by curve fitting with Equation (12).

The piezoelectric plates were bonded at maximum stress position for the cantilever beam operating in second mode. The piezoelectric plates were made from Pb $(Zn_{1/3}\ Nb_{2/3})O_3$-$PbTiO_3$ (PZN-PT) single crystals ($d_{31}$ mode). The crystals were synthesized using the modified flux growth technique. Detailed processing steps have been mentioned somewhere else (Zhang et al., 2004). Synthesized crystals were oriented using Laue technique in TE mode (110/001) and machined to the required dimensions. Machined crystals were electroded by sputtering gold and poled by applying DC field of 2 kV/mm. The area of the single crystal plates was of the order of $7 \times 5\,\text{mm}^2$ while the thickness was in

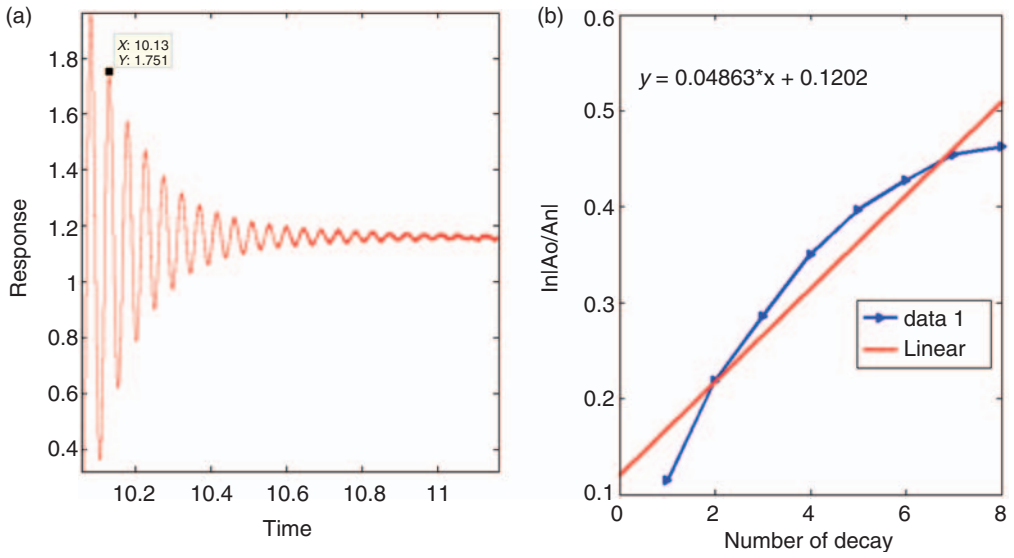


***Figure 4.*** *(a) Step response of the cantilever beam, and (b) the ratio of decaying amplitude.*

the range of 0.7–0.9 mm. Impedance spectrum of each single crystal plate was measured before mounting on the cantilever and after finishing the vibration test. Figure 5 shows the spectrum after the test was finished. It can be seen from this figure that there is significant spurious in the spectrum which was not present before the test. These spurious could be related to two issues (i) damping of the resonance due to epoxy bond between the plate and the beam, (ii) depoling of the crystals after undergoing the vibration test. The crystals were checked for any kind of mechanical damage after the test and none was found to occur. The magnitude of $-d_{31}$ computed from the impedance plots was found to be in wide range of 200–500 pC/N which was about 50% smaller than the starting magnitude. This decrease is believed to be related to depoling effect after exposure to high g-forces. The magnitude of $k_{31}$ computed from Figure 5 was in the range of 0.48–0.53 for all the samples.

The top and bottom row of PZN-PT plates were connected in parallel as shown in Figure 1. A resistance of 3.3 MΩ was connected between terminals and the voltage was recorded by an automated data acquisition system of National Instruments (NI 9215 and NI 9263). The data acquisition system includes a four channel slot, laptop, and Labview program. An accelerometer was mounted near the tip of the magnet. The device was excited at the clamped end of beam where the mass was not attached using a mini-shaker. The shaker acceleration as well as frequency was varied by changing the input voltage and frequency on the function generator via high power amplifier. The experimental set up is shown in Figure 6. The magnetic field of the permanent magnet was measured by a microprocessor controlled Gaussmeter MG-10D (Walter LDJ Scientific Inc.) and was found to be of the order of 0.4T.

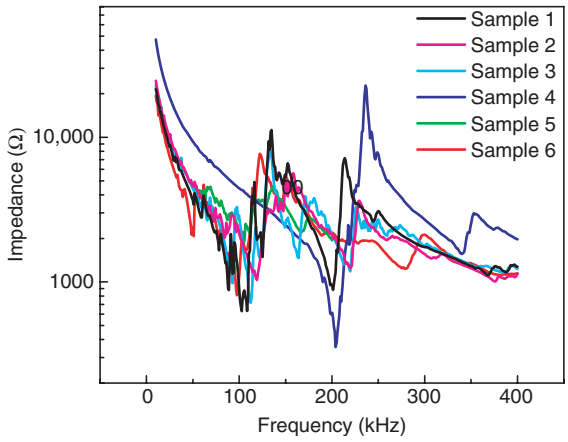


***Figure 5.*** *Impedance spectrum of the piezoelectric single crystal plates after the test. In this figure sample 1 = crystal on top end closer to tip mass; sample 2 = crystal on top in the middle; sample 3 = crystal on bottom end closer to tip mass; sample 4 = crystal on bottom in the middle; sample 5 = crystal on top farthest from tip mass; and sample 6 = crystal on bottom farthest from tip mass.*

The accelerometer used was a piezoelectric shear accelerometer with sensitivity of 9.88 mV/g. The electromagnetic coil was wound around a 'v groove rim' of 7.5 mm inner radius and 12.5 mm outer radius. The number of turns was 500 and the wire gauge was 28 AWG. The measured self inductance (Le) of the coil was 12 mH.

## RESULTS AND DISCUSSION

The output power from the electromagnetic and piezoelectric systems was measured separately as a function of acceleration and frequency. For measuring the frequency dependence, the device was subjected to

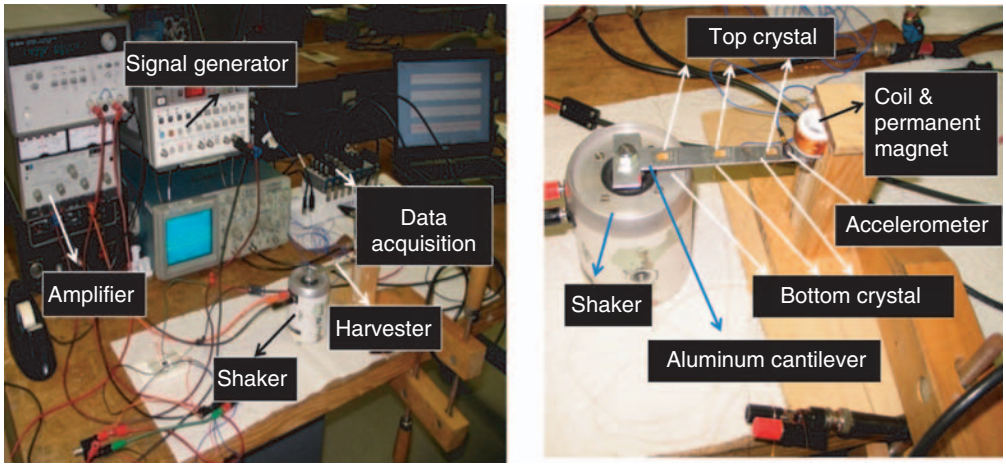


***Figure 6.*** *Picture of the experimental setup (a) connection for data acquisition, power supply and amplifier, and (b) mounting of the device on shaker.*

vibration by applying constant voltage to the shaker and varying the frequency. The first resonance frequency of the beam was found to be 20 Hz which is very close to that predicted from simulations. In this case, the output power of electromagnetic coil across a resistive load of 120 Ω was found to be 8.3 mW. The output power of samples 1 and 2, and samples 4 and 5 across a resistive load of 3.3 MΩ was found to be 19 and 15 μW respectively. Sample 6 generated power of the order of 120 μW in the first resonance mode. The practically observed second natural frequency was 300 Hz. At this operating frequency, the output power from electromagnetic coil reduced to 3.1 μW. The output power from samples 1 and 2 increased to 60 μW whereas sample 4 and 5 reduced to 14 μW respectively. Figure 7(a) and (b) shows the frequency dependence of output power from electromagnetic and piezoelectric systems.

The optimum resistive load for piezoelectric system was selected by measuring the variation of the output power as a function of external load. At the operating frequency of 22 Hz the matching load for the top and bottom rows of PZN-PT (Samples 1 and 2; and Samples 3 and 4) can be determined to be: $R = 1/(2\pi fc) = 5.5\,\Omega$ by using the capacitance magnitude of 1.277 nF. At the second resonance frequency the magnitude of the optimum load will be reduced by an order of magnitude. Thus, a value of 3.3 MΩ which is in between these two extremes was selected for the piezoelectric case to be consistent in the measurements over a whole range of frequency and acceleration. The variation of the output power as function of load at the first resonance frequency is shown in Figure 8(a) and (b). There is a drastic difference in the magnitude of matching load for electromagnetic and piezoelectric case. This presents difficulty in combining the output power from the two mechanisms and would require separate converter circuits.

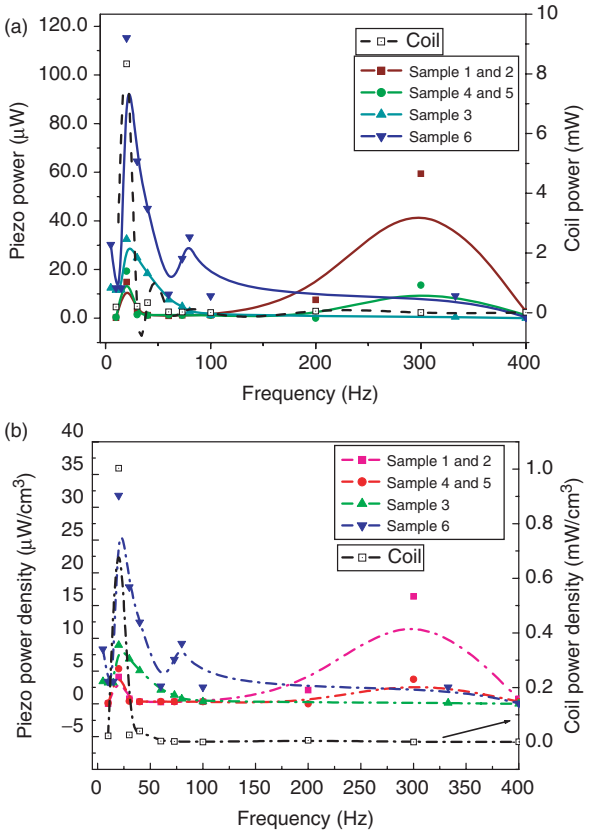


***Figure 7.*** *(a) Output power as a function of frequency from the electromagnetic and piezoelectric system, and (b) power density considering the total system volume from electromagnetic and piezoelectric systems.*

The analytical model for electromagnetic system has been derived in (Poulin et al., 2004) and the expression for output power was found to be as:

$$P_e = \frac{(R_L)(BL)^2 F^2}{2|(Z_e(jw) + R_L)(Z(j\omega)) + (BL)^2|^2} \qquad (13)$$

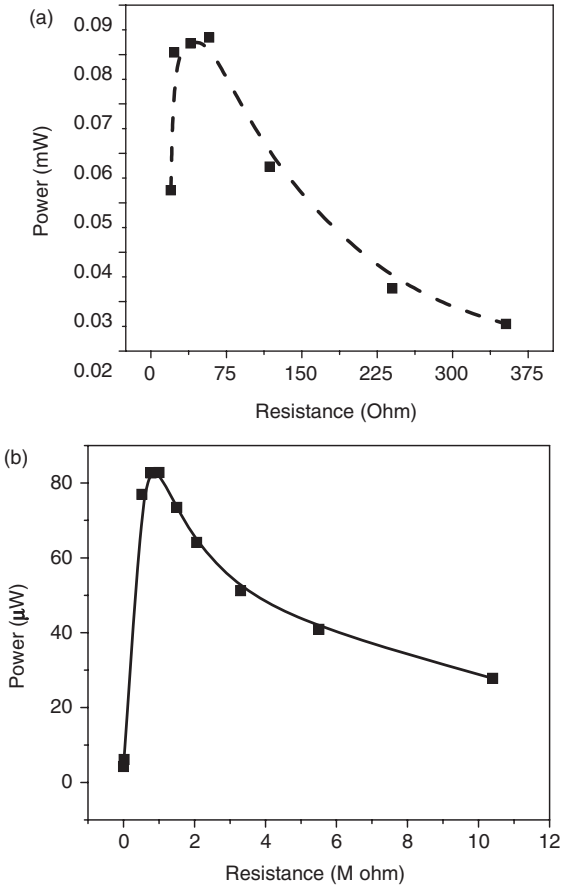


***Figure 8.*** *Variation of ouput power as a function of resistive load (a) electromagnetic, and (b) piezoelectric.*

where $R_L$ is the load resistance, $B$ is the magnetic field, $L$ is the length of coil, $F$ is applied force on the oscillating proof mass, $Z_e$ is the complex electrical impedance given by $z(jw) = Re + Lejw$, $Z$ is the corresponding mechanical impedance of the system, $z(jw) = Mjw + C + K/jw$. The equation was derived based on electromechanical analogy between force and velocity to that of voltage and current. Further, in the above expression $Re$ is the coil resistance, $Le$ is coil inductance, $M$ is total proof mass, $C$ is damping constant, $w$ is operating frequency, j is complex variable and $K$ is spring stiffness. The parameters measured for our device are: $R_L = 120\,\Omega$, proof mass $m_b = 17.6$ gm, mass of the beam $M_b = 6.8$ gm, $B = 0.4$T, length of coil $L = 2\pi rn = 36.7$ m (where r is the mean radius of the hub = 12 mm, and n is number of turns), $Re = 29.3\,\Omega$, $C = 0.045$, and $Le = 13.56\,\mu$H. The stiffness magnitude was calculated using the expression: $K = (3EI)/(L^3)$, where $I = (1/12)bh^3$, b is the width of beam (= 12.5 mm), and h is thickness of the beam (=1 mm). The beam material used was aluminum with Young's modulus of $E = 70$ GPa. Figure 9 shows the plot of Equation (13) along with the experimentally measured values for output power. The maximum in the output power was found to be in close vicinity from both theory (~15 Hz) and experiment (~20 Hz).

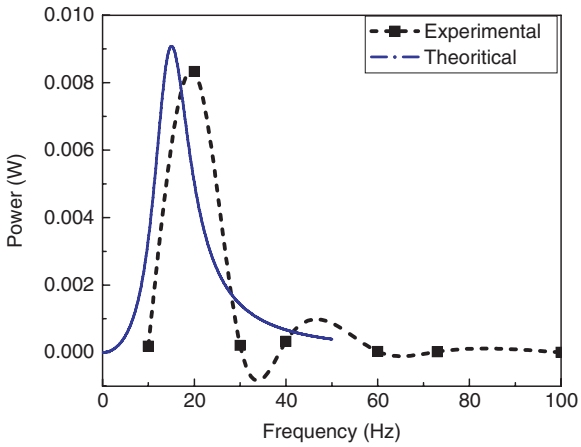


***Figure 9.*** *Theoretical and experimental output power of the electromagnetic coil as a function of frequency. The acceleration magnitude was kept constant in this figure at ≈1 g.*

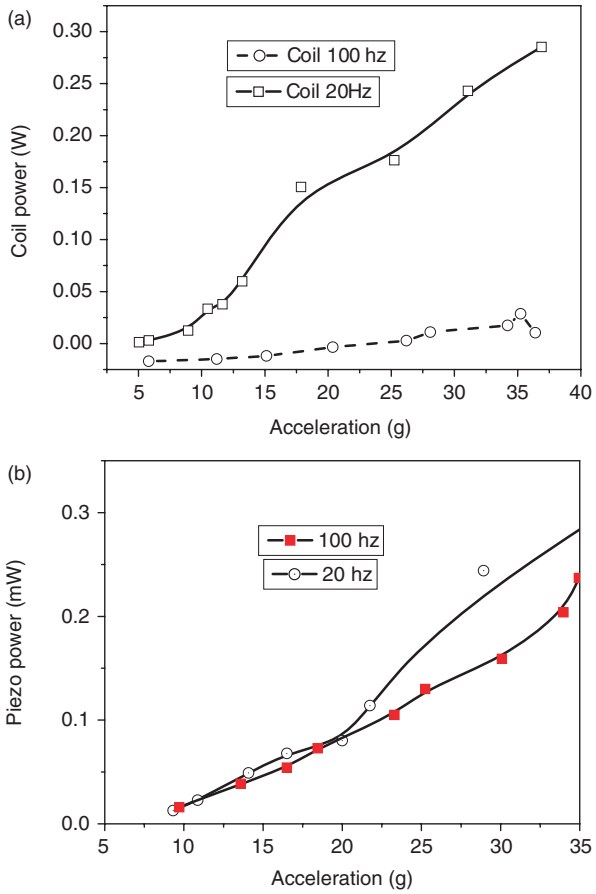


***Figure 10.*** *Power output of (a) PZT (left) and (b) electromagnetic coil (right) for various acceleration and two frequencies (mechanical resonance and nonresonance condition).*

The output power of both the coil and piezoelectric crystals for various acceleration magnitudes are shown in Figure 10 for two different excitation frequencies of 20 and 100 Hz. It can be seen from this graph that the maximum power was measured at 35 g acceleration and 20 Hz frequency with 0.25 W from the coil and 0.25 mW from

the piezoelectric plates. Higher acceleration measurements were not possible because of delamination problem. The power density of the piezoelectric system was calculated from the ratio of power at each crystal to the total useful volume of support structure. To exemplify, for sample 1 the total volume was taken to be as the volume of cantilever, the magnet and the volume of the crystal itself. In the electromagnetic case, the total volume is sum of the volume of coil, the magnet and the cantilever beam. The volume of electromagnetic system and the piezoelectric system were calculated to be 8.3106 and 3.6231 $cm^3$ respectively. These results clearly demonstrate a high power density over a wide frequency range can be achieved by combining the piezoelectric and electromagnetic modalities.

## CONCLUSION

This study reports the experimental and theoretical results on a multimodal energy harvester that combines piezoelectric and electromagnetic mechanism on same platform to enhance the efficiency of mechanical energy harvesting. It was found that the electromagnetic system generates high output power at low frequency, while piezoelectric generates higher power at higher frequency. Thus, combining the two systems together improves the functionality of device over a wide frequency range. The prototype device can harvest a power of 0.25 W and 0.25 mW from electromagnetic coil and piezoelectric system. The overall size of the prototype device was $25 \times 30 \times 125\,mm^3$.

## ACKNOWLEDGMENTS

The authors gratefully acknowledge the support from Texas Advanced Research Program and Office of Naval Research (N00014-08-1-0654).

## REFERENCES

Anton, S.R. and Sodano, H.A. 2007. "A Review of Power Harvesting using Piezoelectric Materials (2003–2006)," *Smart Mater. Struct.*, 16:R1–R21.

Blevins, R.D., 1979. *Formulas for Natural Frequencies and Mode Shape*, Robert E. Krieger Publishing, Malabar, Florida, USA.

Erturk, A. and Inman, D.J. 2008. "On Mechanical Modeling of Cantilevered Piezoelectric Vibration Energy Harvesters," *J. Intell. Mat. Syst. Struct.*, 19:1311–1325.

Kim, H., Priya, S., Stephanou, H. and Uchino, K. 2007. "Consideration of Impedance Matching Techniques for Efficient Piezoelectric Energy Harvesting," *IEEE Trans. Ultrason. Ferroelec. Freq. Cntrl.*, 54:1851–1859.

Laura, P.A.A., Pombo, J.L and Susemihl, E.A. 1974. "A Note on the Vibration of Clamped-free Beam with a Mass at the Free End," *J. Sound Vib.*, 37(2):161–168.

Poulin, G., Sarraute, E. and Costa, F. 2004. "Generation of Electrical Energy for Portable Devices Comparative Study of an Electromagnetic and Piezoelectric System," *J. Sens. Actuators,* A116:461–471.

Priya, S. 2007. "Advances in Energy Harvesting Using Low Profile Piezoelectric Transducers," *J. Electroceram.*, 19:165–182.

Priya, S., Popa, D. and Lewis, F. 2006. "Energy Efficient Mobile Wireless Sensor Networks," *ASME Congress* 2006, Nov. 5–10, Chicago, Illinois, IMECE2006–14078.

Priya, S. 2005. "Modeling of Electric Energy Harvesting Using Piezoelectric Windmill," *Applied Phys. Lett.*, 87, 184101 (3 pages).

Rabaey, K. and Verstraete, W. 2005. "Microbial Fuel Cells: Novel Biotechnology for Energy Generation," *Trends in Biotechnology*, 23:291–298.

Raghunathan, V., Kansal, A., Hsu, J., Friedman, J. and Srivastava, M. 2005. "Design Considerations for Solar Energy Harvesting Wireless Embedded Systems," In: *4th IEEE, Int. symposium on Information Processing in Sensor Networks*, April 25–27, UCLA, Los Angeles, California, pp. 457–462.

Sodano, H., Inman, D.J. and Park, G. 2004. "A Review of Power Harvesting from Vibration Using Piezoelectric Materials," *Shock Vib. Digest*, 36:197–205.

Williams, C.B. and Yates, R.B. 1996. "Analysis of Micro Electric Generator for Micro-electric Generator for Microsystems," *J. Sens. Actuator*, A 52:8–11.

Zhang, S., Lebrun, L., Randall, C.A. and Shrout, T.R. 2004. "Growth and Electrical Properties of (Mn,F) co-doped $0.92Pb(Zn_{1/3}Nb_{2/3})O_3$–$0.08PbTiO_3$ single crystal," *J. Crystal Growth*, 267:204–212.